Spring 5-1-2014

STUDY OF EDGELESS TIMEPIX PIXEL DEVICES

Dylan G. Hsu

STUDY OF EDGELESS TIMEPIX PIXEL DEVICES

A Capstone Project Submitted in Partial Fulfillment of the Requirements of the

Renée Crown University Honors Program at Syracuse University

Dylan G. Hsu

Candidate for B.S. Degree and Renée Crown University Honors

May 2014

Honors Capstone Project in Physics

Capstone Project Advisor: _____

Capstone Project Reader: _____

Honors Director: _____

Date: May 6, 2014

ABSTRACT

Silicon micropattern devices are crucial components of detector systems designed to study decays of exotic subatomic particles containing beauty and charm quarks. Among the technologies under consideration for use in future particle physics experiments are edgeless silicon pixel detectors. In these devices a state-of-the-art fabrication process is used to create sensors with a nearly full active area, as compared to conventional sensors which have a "guard ring" which is a dead region at the sensor periphery. Prototypes used for the study described in this paper were designed and fabricated by VTT Technical Research Centre of Finland. In a test beam study, we find that these devices perform in accordance with expectations and fulfill the technical needs of their intended implementation. This active edge technology is indeed efficient in maximizing the useful area of the sensor. More broadly, these devices meet the needs of a detector for particle physics, and may also find a role in medical imaging or X-ray spectroscopy.

CONTENTS

EXECUTIVE SUMMARY

My Capstone Project is a scientific assessment of a new type of detector for use in experimental particle physics. In this field, a large team of scientists typically designs a large experimental apparatus comprising several types of individual detector devices, a data acquisition system, and data processing software. The purpose of this detector system is to measure and record information on the sub-nuclear particles produced in the energetic proton-proton collisions produced at a particle accelerator. An amount of data taken during a run of extended duration constitutes a holistic data set, which is studied by a multitude of researchers with the goal of confirming theoretical expectations or observing new physical processes. The quality of the resulting physics analysis depends on the design and performance of the individual detectors, the triggering scheme, the amount of data taken, and the resulting experimental uncertainties derived from the apparatus and the analysis procedures. Thus, particle physicists take on a variety of roles in investigating new analysis methods, and designing or building the next generation of detectors. Meanwhile, outside experts such as engineers and manufacturers often contribute to this massive and multifaceted effort. The work I have done serves as a substantive contribution to the ongoing effort to design more effective detectors for particle physics experiments.

The High-Energy Physics Group at Syracuse University is one of several groups around the world which collaborates on the LHCb experiment. LHCb is one of four main experiments at the Large Hadron Collider (LHC) at CERN (the European Organization for Nuclear Research) located in Geneva, Switzerland. LHCb is specifically intended for the study of the decays of beauty-flavored hadrons and other exotic particles, which the LHC's proton-proton collisions are

capable of producing in great numbers. In particle physics, B-mesons are a species of particle composed of a quark and an anti-quark: a bottom quark plus an up, down, strange, or charm anti-quark (the latter being the antimatter version of a quark). The decay of B-mesons are particularly revealing in the study CP-symmetry, a discrete and fundamental property of the basic forces governing the universe. CP symmetry gives that the basic laws of physics are invariant under the compound operation of mirror inversion plus a change of particle to anti-particle. However this symmetry's main importance is held by its breaking, called CP violation, which although very tiny, is one of the essential ingredients in our understanding of the stable matter universe that we experience today. The Big Bang created equal amounts of matter and antimatter, but this now seems quite preposterous, since we see a preponderance of matter over antimatter in the observable Universe. This is the basic reason why CP violation must be explored and understood. While the Standard Model of particle physics incorporates CP violation, the parameters which quantify its role in particle interactions are not known with satisfactory experimental precision. Furthermore, it is possible that aspects of the model are wrong, and "new physics" may be found.

The LHCb experimental apparatus consists of several detector devices which serve in studying the aforementioned physics by specializing in measuring different characteristics of the particles produced in proton-proton collisions. Altogether, the apparatus gathers information about the identity, trajectory, momentum and energy of those particles produced, and can identify individual particles of interest from the billions spraying out from the collision point. The first line of detection is the Vertex Locator, or VELO, which constitutes about 40 planes of silicon detectors only 8 mm from the beam pipe. As exotic particles and their decay products pass through these detectors, a 3-dimensional "electronic

photograph" is taken of the process, providing information about the decays which physicists aim to study. A better detector would provide more accurate and useful information for the analysis; this is the one of the motivations behind the LHCb Upgrade project. Numerous devices for future generations of the tracking system have been under consideration for some time, including silicon strip detectors, silicon pixel detectors, and diamond detectors. I will omit a discussion of the advantages and drawbacks of these various types of detectors and instead henceforth focus on the particular candidate device which I have studied, namely edgeless silicon pixel detectors.

Prior generations of silicon detectors have been designed with a dead region at the periphery which cannot serve in detection. The purpose of this dead region is to host a "guard ring" which maintains a regulated voltage drop between the active region and the detector edge for stable operation. The prototype devices which I have studied are revamped silicon pixel detectors which feature a very small inactive region at the edge, designed by VTT Technical Research Centre of Finland. The reduced edge means that in a plane featuring an array of many such devices, a higher proportion of the planar area is active in tracking particles. The necessary overlapping would also be reduced, minimizing unwanted material effects. For an idea of scale, these devices have a size of about 1.4 cm x 1.4 cm, with an edge region of less than 0.1 mm. The active part of the device comprises a 256 x 256 matrix of pixel detectors, each only 55 μm in size.

The main test of these devices was conducted in a particle beam at CERN in 2012. The test beam setup consists of several pixel detectors in parallel which serve as reference, with the device under test in the middle. A pion particle beam is directed through all of the devices, each of which individually provides

detection information that is used to calculate the tracks of individual particles. Using this data in the analysis, we learn much about the performance of the detector. A central measure of the quality and accuracy of the device is the spatial resolution, which comes on the order of micrometers. This quantifies the precision with which the device locates particles passing through. The procedure for ascertaining the resolution is as follows. During data taking, the beam particles register a hit on each device in the test setup. Sometimes the particle deposits charge in more than one pixel, which is handled algorithmically as a hit cluster (otherwise it is a 1-pixel cluster). When this data is analyzed, tracks are fitted through the hit clusters which approximate the trajectories of the incident particles. The residual of a fitted track is calculated by taking the difference between the position of the associated hit on the device under test and the position where the fitted track intercepts the device. Through fitting a high number of tracks, the residual forms a distribution which is somewhat normal. The standard deviation of this residual distribution constitutes the spatial resolution.

The algorithm used to determine the position of a hit cluster is important in determining the resolution. While a 1-pixel hit cluster only carries information about the amount of charge deposited in a single pixel, a 2-pixel hit cluster carries this information for the 2 adjacent pixels. This means that the relative amount of charge deposited in the pixels constituting the cluster can be used to more accurately estimate the place where the particle actually hit the device. Various algorithms are discussed in the scientific literature for optimizing the resolution using different formulae to relate the charge deposition topology to reconstructed spatial coordinate.

Beyond the mathematics of the problem, there is an electronics concern rooted in the fact that for a particular device, there may exist a nonlinear relationship between the charge deposited in a pixel and the signal read out. Thus, a charge calibration which accurately quantifies this relationship allows non-linear charge weighting and can theoretically improve the calculation of hit position for multiple-pixel clusters as previously described—and improve the spatial resolution. This was largely outlined in a 1993 paper by R. Turchetta. Since the accuracy of determining the hit position differs depending on cluster sizes, there is an angular effect noted in Turchetta's paper. In brief, a beam of incident particles at perpendicular incidence will create a large number of 1-pixel clusters with some 2-pixel clusters as well. However, if the device is rotated slightly so that the beam is no longer perpendicular to the device, the paths of the individual particles are more likely to span pixels whilst traversing the detector, creating a preponderance of 2-pixel clusters. As the angle is increased further, one begins to see the 2-pixel clusters supplanted by more 3- and even 4-pixel clusters. Algorithmically, 2-pixel clusters are optimal for accurately determining the hit positions, so the spatial resolution is optimized at an angle of incidence where 2-pixel clusters dominate the most. As such, an important part of my study was determining the spatial resolution as a function of angle to find this optimum point.

The two devices I studied both exhibited a local minimum in the spatial resolution at a moderate angle of incidence close to that predicted for their particular geometry. The resolution performs identically in the horizontal and vertical directions of the chip at normal incidence, but the dependence on angle was only investigated in the horizontal or X direction. After using a charge calibration taken by colleagues at NIKHEF in Amsterdam, and applying further

empirical corrections to the cluster algorithms, the resolution improved substantially. For one device, F08-W0171, the improvement in resolution at a particular threshold was shown to be from 5.56 μm to 5.05 μm. By comparison, the individual pixels are 55 μm wide.

A noted concern with these prototype edgeless sensors is potential distortion effects which may appear near the edge of the active region. Prior simulations and analyses by other members of the collaboration give reason to doubt the fidelity of the edge regions. Due to the reduced area of the guard ring, the bias voltage applied across the chip creates a distorted electric field at the edges which creates an artificial dominance of 2-pixel clusters and thus hampers the efficiency of associating hit clusters to tracks. Formally, the efficiency is the ratio of the number of particle tracks associated with hits on the device to the total number of tracks impinging on the device. My study examines the devices' efficiency and functionality at the edges in order to evaluate whether the edge distortion is problematic for possible implementations.

I found that the devices performed very well at the edge, in agreement with concurrent work by our collaborators at NIKHEF. The devices remained near 100% efficiency up to and including the pixels at the device boundary. In both, efficiency dropped significantly only within several micrometers of the edge—well past the last row of pixels. However, we did find confirmation of the aforementioned distortion effect near the edges which adulterates the quality of any clustering algorithm there.

Due to my work analyzing these devices, I conclude that the device performance is accurate and reliable. While my work is a small part of a much larger collaborative effort in the detector physics community, elements of my study serve as an original contribution to the collective knowledge of these state-

of the-art devices. In conjunction with work done by others in the collaboration working with other prototypes, this validates consideration of the use of “edgeless” silicon detectors for particle physics experiments. In addition, such devices may find a future in medical imaging and X-ray crystallography (which have historically been dominated by silicon strip detectors). Principally, the advanced properties of these detectors place them at the forefront of experimental detector technology, with the potential to provide to physicists the data of tomorrow.

1 THEORETICAL MOTIVATION

The LHCb experiment is dedicated to the experimental study of heavy flavor physics at the Large Hadron Collider (LHC), the world’s highest energy accelerator located at CERN (the European Organization for Nuclear Research) in Geneva, Switzerland. The primary purposes of LHCb are to observe interesting decay modes of two types of fundamental sub-nuclear particles: beauty and charm hadrons, and to find evidence of new physics. One of the possible manifestations of new physics is the uncovering of new sources of CP violation. CP violation is an important question which must be addressed: the scientific community has no complete explanation for why the universe is populated by a disproportionate amount of matter, while antimatter is virtually nonexistent. After the Big Bang a situation where matter and antimatter were present in equal quantities evolved in the current matter-dominated universe. An essential ingredient for this transition is CP violation. In the current understanding of the subatomic particle interactions (the Standard Model) CP violation is incorporated in the so-called CKM matrix. However this source of CP violation is

too small to explain the baryon excess in the current universe. Thus new sources of CP violation are expected. In general, new physics is expected to manifest itself in flavor physics, and there are strong theory motivations to expect deviations from standard model expectations in beauty and charm decays. The reason LHCb was proposed to explore this rich phenomenology in search of clues that can lead us to a deeper understanding of CP violation.

The CKM mechanism is the Standard Model's parameterization of flavor-changing weak decays of quarks.[1] This matrix is unitary, and thus for 3 generations of quarks it encompasses 4 independent parameters, one of which describes CP violation in the quark sector:

$$\begin{pmatrix} \boldsymbol{d'} \\ \boldsymbol{s'} \\ \boldsymbol{b'} \end{pmatrix} = \begin{pmatrix} \boldsymbol{V_{ud}} & \boldsymbol{V_{us}} & \boldsymbol{V_{ub}} \\ \boldsymbol{V_{cd}} & \boldsymbol{V_{cs}} & \boldsymbol{V_{cb}} \\ \boldsymbol{V_{td}} & \boldsymbol{V_{ts}} & \boldsymbol{V_{tb}} \end{pmatrix} \begin{pmatrix} \boldsymbol{d} \\ \boldsymbol{s} \\ \boldsymbol{b} \end{pmatrix}. \quad (1)$$

The charged current interactions couple each up-type quark [(u)p, (c)harm, and (t)op] with a linear combination of down-type quarks [(d)own, (s)trange, and (b)ottom]. Furthermore, by properties of unitary matrices,

$$\boldsymbol{V_{ij}\,\overline{V_{jk}} = \overline{V_{\imath j}}\,V_{jk} = \delta_{ik}}\,, \quad (2)$$

where δ_{ik} represents the identity matrix and $\bar{z}$ is the scalar complex conjugate of z. Existing analyses of experimental data offer a fairly sturdy determination of the CKM matrix elements:

$$|\boldsymbol{V_{ij}}| = \begin{pmatrix} \boldsymbol{0.97427 \pm 0.00015} & \boldsymbol{0.22534 \pm 0.00065} & \boldsymbol{0.00351^{+0.00015}_{-0.00014}} \\ \boldsymbol{0.22520 \pm 0.00065} & \boldsymbol{0.97344 \pm 0.00016} & \boldsymbol{0.0412^{+0.0011}_{-0.0005}} \\ \boldsymbol{0.000867^{+0.00029}_{-0.00031}} & \boldsymbol{0.0404^{+0.0011}_{-0.0005}} & \boldsymbol{0.999146^{+0.000021}_{-0.000046}} \end{pmatrix}. \quad (3)$$

A significant portion of current effort in analyzing data from LHCb is devoted toward an accurate parameterization of the CKM mechanism. The unitarity of the CKM matrix allows the construction of a unitary triangle based on

its matrix elements. In order for the Standard Model to be self-consistent, this triangle must be unitary and hence must close, as seen in **Error! Reference source not found.**.

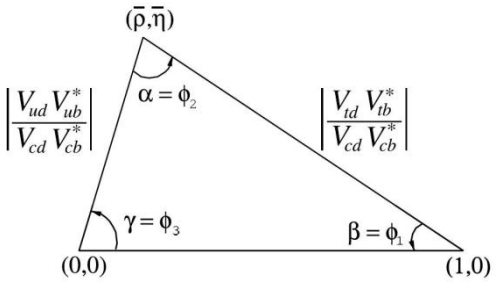

Figure 1.1. Unitary triangle formed from parameters of CKM matrix.

2 THE LHCB EXPERIMENT

Supercolliders such as the LHC produce exotic decays in the debris produced by the proton-proton collisions at high energy. In conjunction with this, an experimental apparatus such as the LHCb detector is needed which captures information about these exotic decays. Such system is placed under many demands and constraints which are summarized to follow. Various detector devices operate synchronously to provide information which allows identification of particles and calculation of their trajectory, momentum, and energy. The quality of the resulting data analysis hinges on the quality of information available from the detector. Huge numbers of events are created during a data-taking run, generating an enormous amount of data that cannot be all processed and stored. A trigger algorithm is needed to filter the “needle in the haystack” which is the useful information. This trigger is crucial and relies on very fast detectors that are the first line of detection for the collider’s products. Each collision produces hundreds of tracks, and there are a few collisions every 50 ns. Most of this data has to be thrown out expediently, requiring sensor devices and front end electronics close to the collision point. This introduces an additional complication in that the experiment generates substantial radiation which damages sensitive

electronics such as particle detectors and computer chips over time. Various teams at collaborating institutions each contribute to specific detector subsystems that collectively make up the monstrous complexity that is the LHCb detector.

The Vertex Locator (VELO) is an important component of the existing implementation of the LHCb detector, the development of which Syracuse University's High-Energy Physics group has been a large contributor. Its purpose is to reconstruct the vertex topology of the events produced in the pp interaction. As beauty and charm are relatively "long lived" quarks, their distinct signature is a displaced vertex. This shows the importance of a precise vertex reconstruction in our experiment. The VELO detector is the closest to the interaction point of the collider, thus it operates in a severe, non-uniform radiation environment, while maintaining spatial precision on the order of 4 μm.[2] The lifetime of the LHCb experiment provides for several upgrades in order to improve the apparatus for higher collider beam energies; considerable effort has gone toward development of detector technologies which could allow us to improve on the VELO for the LHCb upgrade. The criteria for these novel technologies include high spatial precision and resistance to radiation dose over time (radiation-hardness). Among the technologies under consideration are edgeless silicon pixel detectors, silicon microstrip detectors, and synthetic diamond detectors.

2.1 SILICON PIXEL DETECTORS AND THE LHCB VELO UPGRADE

In a silicon detector, a charged particle of sufficient energy passing through the silicon bulk causes ionization. This frees electrons from the silicon atoms; the new electron vacancies constitute a positive charge carrier called “holes.” Typically, about 24,000 electron-hole pairs are produced. A reverse bias across the sensor is applied, causing both charge carriers to drift apart toward collecting electrodes. This induces an electronic signal which can be amplified, and if the electrodes are segmented into pixels, this provides information on where and when the particle traversed the detector.

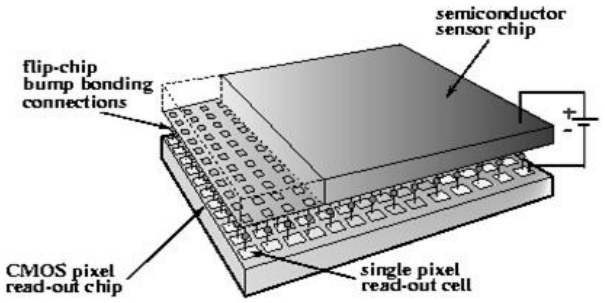

Figure 2.1. Cutaway diagram of a silicon pixel detector.

A study published by R. Turchetta in 1993 examined various tracking algorithms for silicon microstrip detectors, and the associated methods for determining the spatial resolution of the detector.[3] (The spatial resolution serves as a measure of the device’s precision or quality.) The paper, which is relevant for both strip and pixel-based detectors, considers algorithms for incident particles impinging at near-normal angle as well as for larger angles. At near-normal incidence ($\theta = 0°$), the vast majority of hits form 1- or 2-pixel cluster hits on the device by passing through 1 or 2 adjacent pixels and depositing sufficient

charge to be registered as a cluster. Here, 2-pixel clusters are more useful in accurately determining the position of the hit, so the paper theoretically predicts optimal resolution at an angle where 2-pixel clusters are dominant. This local minimum is quoted as

$$\theta_{\mathrm{opt}} = \tan^{-1}\left(\frac{P}{t}\right), \qquad (4)$$

where *P* is the pitch of the device (i.e., the width of the individual pixels), and *t* is the thickness of the detector.

An experimental test of silicon pixel detectors was conducted in 2009 and published in 2011 in order to assess the viability of such devices for use in a future device or upgrade.[4] This prior study established a methodology along with substantial software for evaluating the devices on multiple criteria. The particular devices tested were of the TimePix make, with individual pixels of size 55 x 55 μm, planar size 1.4 x 1.4 cm, and thickness 300 μm. The relevant contributions of the study are the electronics setup of the test bench for data acquisition, calibrations of the device, empirical corrections to the data, and confirmation of the aforementioned relationship between spatial resolution and incident angle. Moreover, the study revealed a best spatial precision on the order of 4 μm, which places these pixel detectors in the same league as the previously mentioned VELO technology. What was *not* detailed in this paper which is very important to the viability of an implementation is the fact that the device design possesses a significant guard ring area at the device periphery where there is no detection capability. This limits the usefulness of an implementation somewhat because the total area of a large plane composed of these devices would suffer from dead regions near the edge of each

constituent device. Hence, this leads to the present study which we have conducted an examination of a new class of pixel detector prototypes that attempt to assuage this problem with a reduced guard ring—so-called "edgeless" sensors.

The prototypes used for the study described in this paper were designed by VTT Technical Research Centre of Finland, whose team developed a state-of-the-art fabrication process to create sensors with a negligible guard ring at the sensor edges.[5] Furthermore the edge is "active" in that it is doped to participate in charge collection. The intention of such a feature is to allow a tile-like arrangement of many of these sensors to create a large-area imaging array for an implementation such as the upgrade to the VELO detector. Preliminary tests done by VTT reveal some strange behavior in the edge regions of these devices such as an increased response in the second-to-last row of pixels near the edge compared to the rest of the chip, and a decreased response in the last row. However, another team reported a "world record" of less than 2 μm-wide region of insensitivity at the edge of the chip for an n-on-n edgeless pixel detector coupled to TimePix readout.[6] This is exactly the class of chip which we chose to study, and that for which we examined in detail the efficiency at the edge.

3 TEST DEVICES

The two test devices which we studied extensively were designated **F08-W0171** and **H08-W0171**. For simplicity we shall refer to them as **F08** and **H08**. These prototype sensors were produced by VTT and share several characteristics.

	F08	H08
Thickness	200 µm	200 µm
Pitch	55 µm	55 µm
Sensor Type	n-on-n	n-on-n
Pixel-to-Edge Distance	55 µm	100 µm, floating guard ring
Predicted Optimal Angle	15.4°	15.4°

Table 1

These devices each saw some travel, having been transported to both Syracuse and NIKHEF for calibration and other tests after the testbeam procedure described in the following section was conducted at CERN in 2011.

4 EXPERIMENTAL METHODS

4.1 THE TIMEPIX TESTBEAM RUN

The test devices of interest to this paper, as well as others, were experimentally tested in 2012 at CERN using a test beam setup. The object of this setup is to evaluate the performance of a detector device using several other position-sensitive devices as reference. The physical apparatus of the test, called the tracking telescope, consists of 9 TimePix reference planes in a parallel arrangement, sandwiched between two scintillators. The reference planes are silicon pixel detectors, from a previous iteration of the TimePix design, with 300 µm thickness; they are mounted on rails such that depending on the test in

question, the distance between the individual devices can be adjusted. This is shown in Figure 4.1. Additionally, various electronics modules assist in generating and recording trigger signals from these devices. A collimated pion beam was used to register hits on the devices for the test. Data is read out from the reference planes using RelaxD data acquisition modules.

We note the following details in the electronics setup for thoroughness. The data-taking operation of the test beam is based on the concept of a shutter. When the two scintillators fire in coincidence, the shutter is opened and the devices begin data taking. Simultaneously, the setup counts the number of scintillator triggers prior to opening, and closes the shutter after either a certain amount of time has elapsed or a certain number of triggers has been received, whichever happens first. During the periods in which the shutter is opened, the devices involved in the telescope test have the capability to take data either in Time-over-Threshold (TOT) mode or Time-of-Arrival (TOA) mode. In TOT mode, the device measures the time interval in which the charge continuously collected from each pixel surpasses (or is “over”) the minimum charge threshold of the device. This may be used to ascertain the amount of charge deposited by a particle passing through one or more pixels. However, there is a nontrivial relationship between TOT information and deposited charge which will be discussed later. In TOA mode, the device measures the time between the previously-mentioned charge threshold crossing and the shutter closing. Together, the reference planes operating in TOT and TOA mode provide an accurate history and location of the tracks of the beam particles. This may be used as a reference for the device under test (DUT): another sensor placed in the middle of the telescope setup on a rotation stage, whose properties we wish to measure. The DUT is operated in TOT mode for intensive study of its

properties. The purpose of the rotation stage was to allow the angle of incidence of the beam on the device under test to vary. This test setup was used to gather the data on which the present analysis on various aspects of the detector was performed.

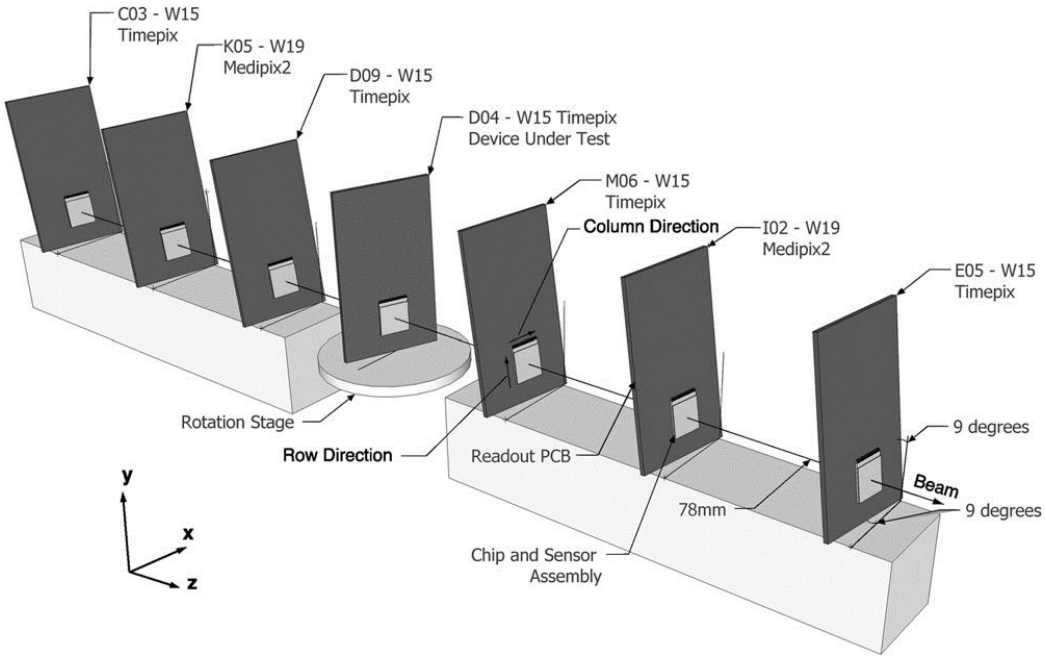

Figure 4.1. Example of device arrangement for the 2011 TimePix test beam setup.

4.2 SPATIAL RESOLUTION

The primary measure of the device performance is the *spatial resolution*. We calculate this as follows: When a constituent particle of the beam passes through the telescope, it registers a hit on each device of the telescope. This is detected by creating an electronic signal in one or more pixels of the silicon pixel array of each device. The software written to analyze this data reconstructs particle tracks through these hits on the reference planes. Next, these tracks are

projected onto the device under test and the location where the tracks impinge on the device under test is calculated. The software then attempts to match these tracks with hits on the device under test by pairing hits with nearby impinging tracks. The difference between the hit position and the projected track intercept on the DUT in the horizontal (**x**) or vertical (**y**) direction constitutes the residual in **x** or **y** for that particular association. With many hits, the residuals form a distribution; the standard deviation of this distribution defines the spatial resolution in **x** or **y** for the device. That measures how well the incident track can be localized. Using the rotation stage, data was taken over a range of angular values for the two test devices to determine the relationship of spatial resolution versus incident angle.

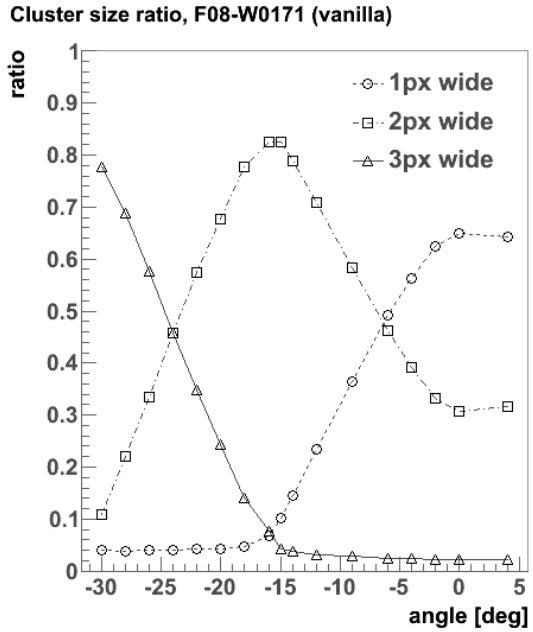

Figure 4.2. Cluster width in X as a function of angular orientation for F08 device.

Because the rotation stage itself is subject to some measurement error, a method was established in the prior study for determining the absolute 0-degree angle. In other words, there may be some intrinsic angular offset which must be

accounted for when examining the resolution as a function of angle. The method used to determine this intrinsic offset relies on the known relationship between angle of incidence and cluster width. For example, as the angular rotation of the device in **y** is increased, a beam particle will on average cross more pixels as it traverses the device, thereby creating hit clusters with a greater width in **x**. The proportion of hit clusters of different widths changes with angle; its shape can be examined for where 1-pixel-wide clusters appear the most to determine the intrinsic offset, as shown in Figure 4.2.

The prior study established that there exists a nonlinear relationship between the amount of charge collected from a pixel in the detector and the corresponding response of the electronics. While the devices are expected to perform reasonably well when this relationship is assumed to be linear, it was shown previously that the device resolution can be improved through a charge calibration which quantifies this nonlinear relationship for the device. This calibration is performed by using a purely electronic setup to pass test pulses of varying amount to the individual channels of the device (65,536 in all) and reading out the response. In theory, a separate calibration curve could be fit to data for each individual channel, which would most accurately calibrate the data obtained from the test beam for calculating the residuals. However, there are several issues with this approach. Fitting 65,536 curves is extremely computationally expensive. Moreover, an actual implementation of such devices would comprise a substantial number of sensors which would make this method too prohibitively complicated. Hence, the per-pixel method was discarded in favor of an average calibration which applies a single response function to the entire chip.

To perform the calibration, the test devices were shipped to NIKHEF where, using a test setup, 256 channels evenly spaced across the chip were pulsed. The calibration data for these channels was then averaged together, and a surrogate function fit to this data to obtain the average calibration. The form of the function is

$$f(x) = (gain)x + (ToT_0) + \frac{c}{x-T}\ , \qquad (5)$$

where gain, ToT_0, c, and T are parameters. As a small correction, when performing the fit the function is convolved with a Gaussian to account for electronic noise in the channel

$$\boldsymbol{g(x) = \left((gain)x + (ToT_0) + \frac{c}{x-T}\right) * \left(\frac{1}{\sigma\sqrt{2\pi}} exp\left(-\frac{x^2}{2\sigma^2}\right)\right)\ .} \qquad (6)$$

The surrogate function fit to the data for the H08 device is shown in Figure 4.3**.**

One concern with the charge calibration was whether the channel response was more or less the same for different channels. In order to address this concern, we fit each of the 256 tested channels with the surrogate function to observe any variation of the calibration parameters across the chip. The variation among channels proved to be substantial, but we nonetheless confirmed the efficacy of the average calibration across the chip after subsequent corrections were performed.

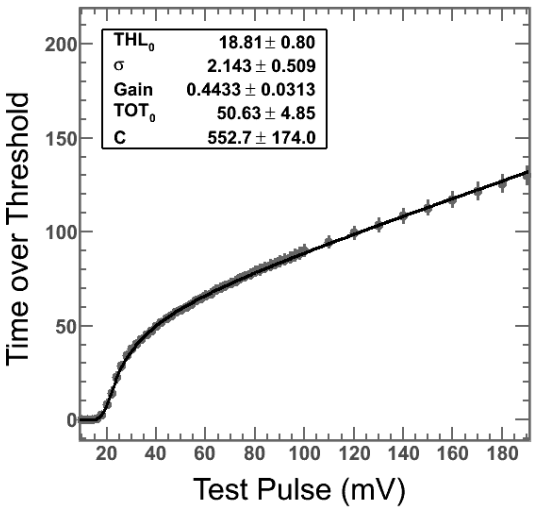

Figure 4.3. Surrogate function fit for the average calibration across the H08 chip.

After the calibration, it is necessary to apply another correction in order to account for non-linear charge sharing. This phenomenon arises due to the physical effects in the detector. Since the pixel size is large compared to the diffusion width of drifting electrons in 200 μm thick silicon, charge sharing among pixels in a hit cluster is imperfect, and this hampers the accuracy of the hit position determination. The charge sharing behavior is captured well in a quantity η, which for our purposes is a 2-dimensional distribution of the calculated position of a hit versus the position of the track with which it is associated. Perfectly linear charge weighting would result in this distribution clustering around a simple linear function. Empirically, this is not what is found. It turns out that the charge offset which is initially unaccounted for prior to charge calibration helps to mitigate the nonlinear η shape, and that after applying the charge calibration the charge sharing actually worsens. Thus, we apply an empirical correction in the following way. First, we identify the necessary correction to the η distribution by fitting a 5^{th}-degree polynomial function to the profile of the *inverse* η distribution from a small sample of the data. An example of this fit is shown in Figure 4.4. Then, this

inverse function is applied to the complementary data, and the resultant η distribution is linear. Once the charge calibration and η-correction have been determined, the benefits of such efforts become clear in the way of an improved spatial resolution, especially at normal incidence.

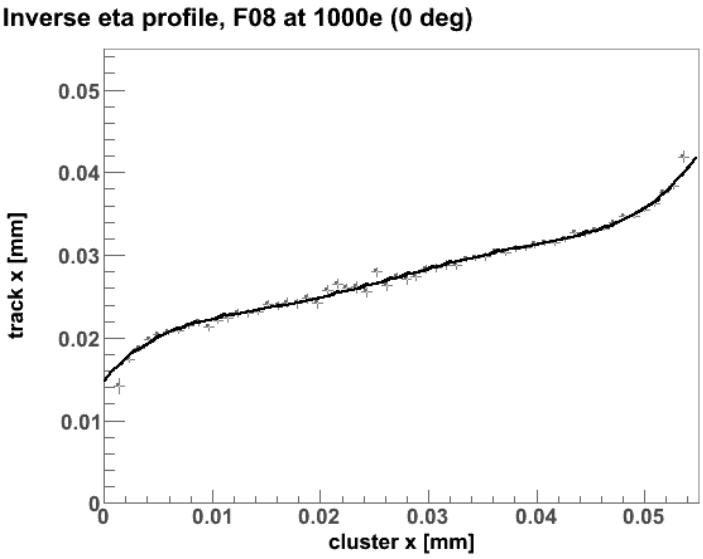

Figure 4.4. Fit to the inverse eta profile for F08 at 1000e threshold to determine the empirical correction.

After the study of the spatial resolution's angular dependence and improvements thereof, the effects of different charge collection thresholds and bias voltages on the performance of the device under test were also studied. For the F08 device, the spatial resolution study was conducted at four different thresholds; for the H08 device, the spatial resolution study was conducted at four different bias voltages.

4.3 EFFICIENCY AT THE SENSOR EDGE

Another important aspect of the test devices which we wish to evaluate is their performance at the very edge of the chip. This is important for evaluating that the usable area of the sensor is maximized. The figure of merit to be used at the edge of the device is the *track-matching efficiency*. In the data taken from the

test beam setup, the device registers many hits whose position is calculated from charge-weighting algorithms. In the domain of a given pixel, there are a number of hits located there. A fraction of these hits are associable with reference tracks; this defines the track-matching efficiency. These are considered “real” hits. When the test beam is focused on the center regions of the device under test, this fraction is nearly 100%. For data runs where the beam is focused at the edge to study the behavior there, we expect a quick drop-off close to the edge, with the key figure being, how close to the edge the device still performs efficiently. We omit a detailed discussion of the reasons for strange behavior at the edge other than the fact that we expect a distorted electric field in the peripheral regions to be partly responsible for these edge effects.

5 RESULTS

5.1 SPATIAL RESOLUTION STUDY

Firstly, we note that the previously discussed calibration and η correction procedures were effective in improving the spatial resolution of the device. The benefit of these corrections to the residual distributions was ubiquitous but most dramatic at normal incidence. The contribution from 2-pixel-width clusters to the overall residual distribution improved the most after applying the corrections. See **Error! Reference source not found.** for an example of the improvement in residuals for the F08 device.

The two test devices have thickness 200 μm and pitch 55 μm, corresponding to a prediction of 15.4° for the local minimum. With both devices, we found a relationship of spatial resolution versus angle of incidence which

qualitatively agreed with the Turchetta prediction. With increasing angle from normal incidence, the resolution improved toward a local minimum on the order of 4 μm in the vicinity of 15°. The charge sharing corrections improved the resolution substantially away from this local minimum, e.g., at normal incidence.

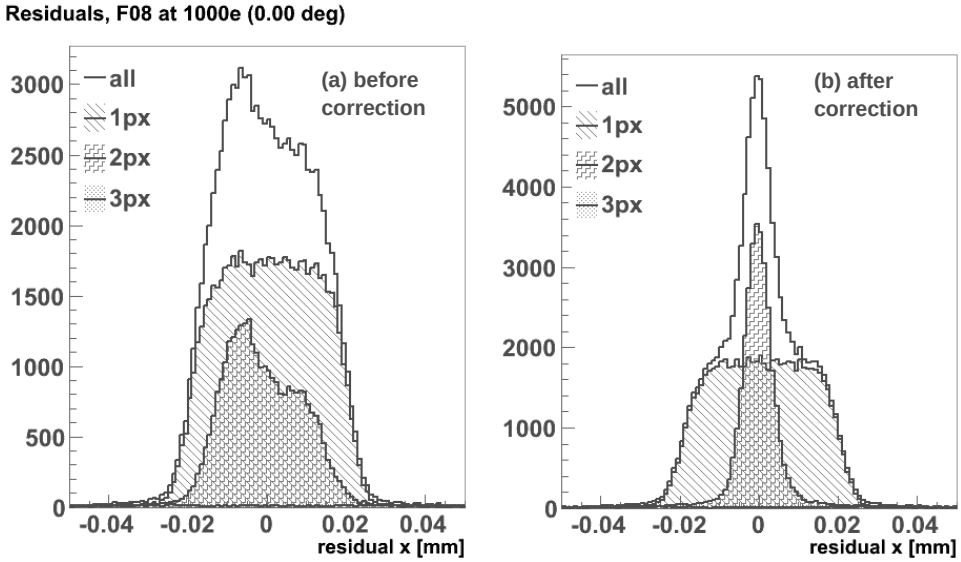

Figure 5.1. Residuals for F08 at normal incidence before and after applying corrections.

For the F08 device, the resolution exhibits this optimal angle at three different thresholds (**750e**, **1000e**, **2000e**), as seen in Figure 5.2. These thresholds signify the minimum number of electrons which must be read out from the device in order to register a hit. The lowest threshold, **750e**, lies very close to the "noise threshold" which is the amplitude of fluctuations caused by purely random noise signals in the electronics. As the threshold is increased to **1000e** and **2000e**, the structure of the angle scan changes little. The data taken at **3000e** did not include as broad an angular range but serves as a sanity check: the magnitude of the resolution near the local maximum at 0° remains constant across the thresholds. For the H08 device, the results are similarly encouraging,

for different biases, and show best spatial resolution on the order of 4 μm. This is indicated in Figure 5.3**.**

F08-W0171, 750e

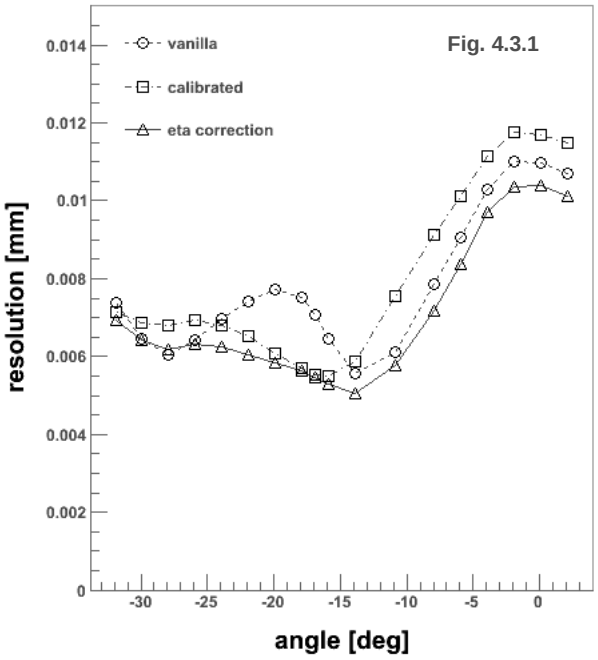

F08-W0171, 1000e

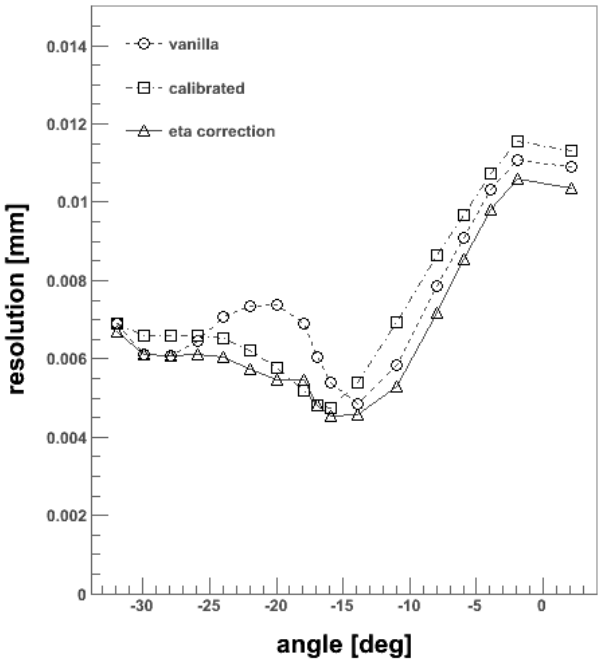

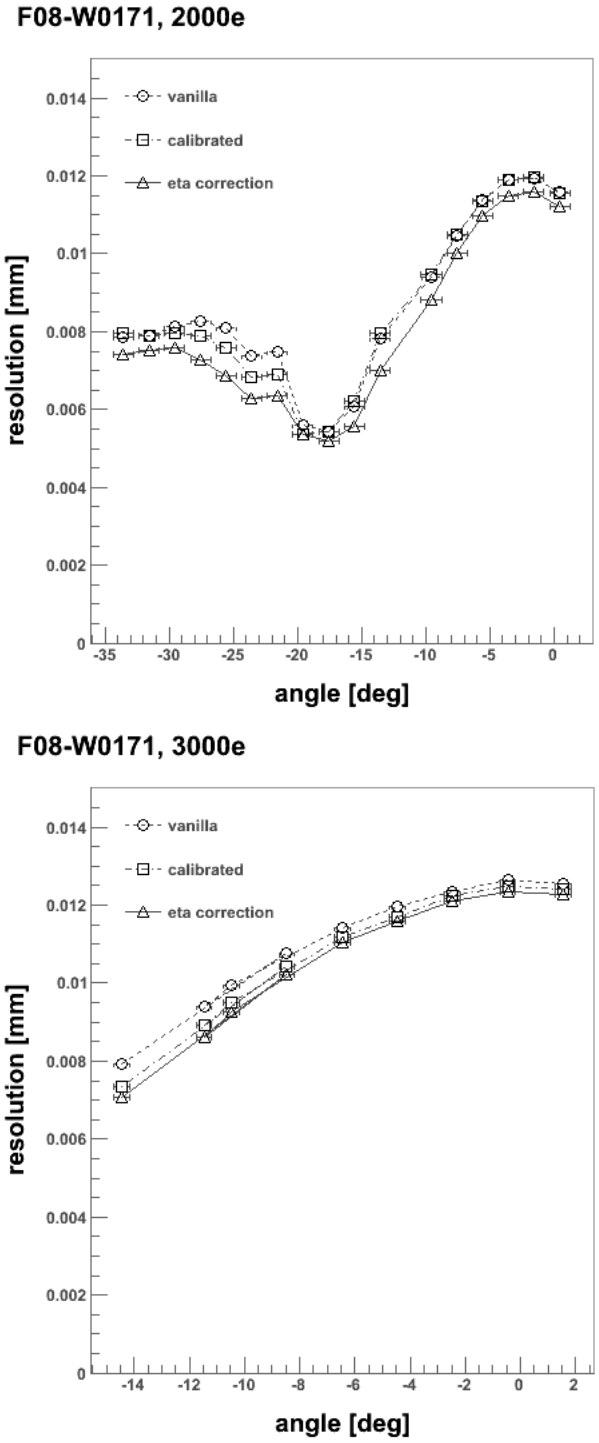

Figure 5.2. Spatial resolution versus angle for the F08 device at four different charge collection thresholds, denoted by the number of electrons: 750e, 1000e, 2000e, and 3000e.

H08-W0171, 1000e, bias -40V

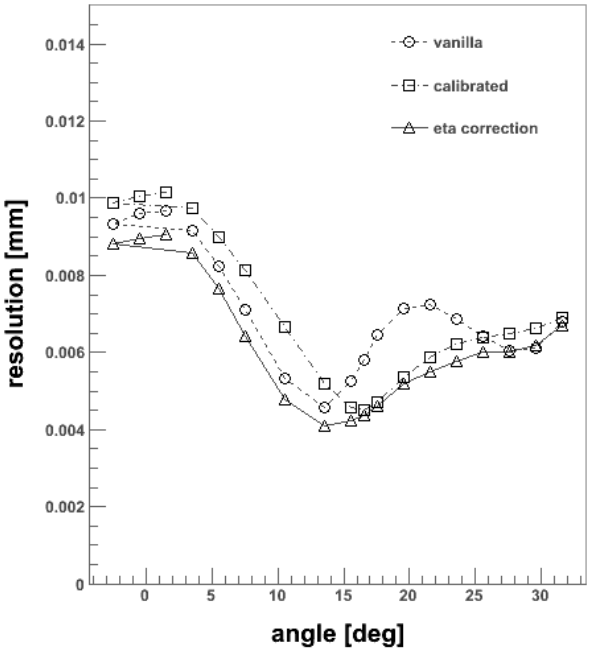

H08-W0171, 1000e, bias -60V

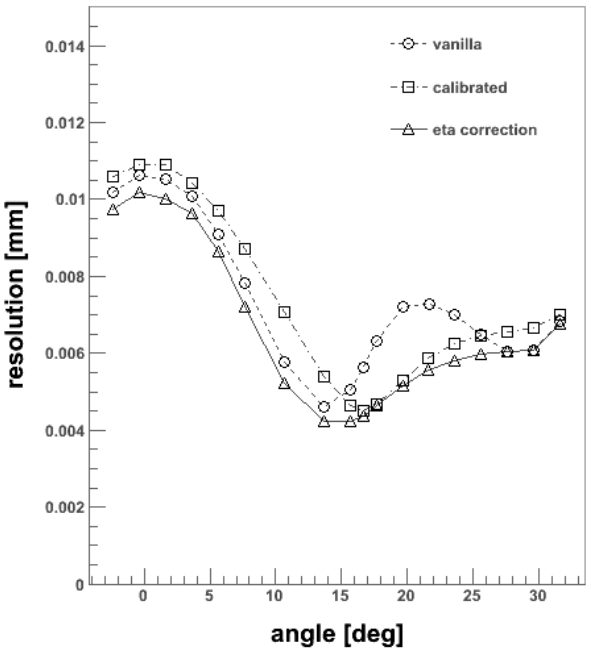

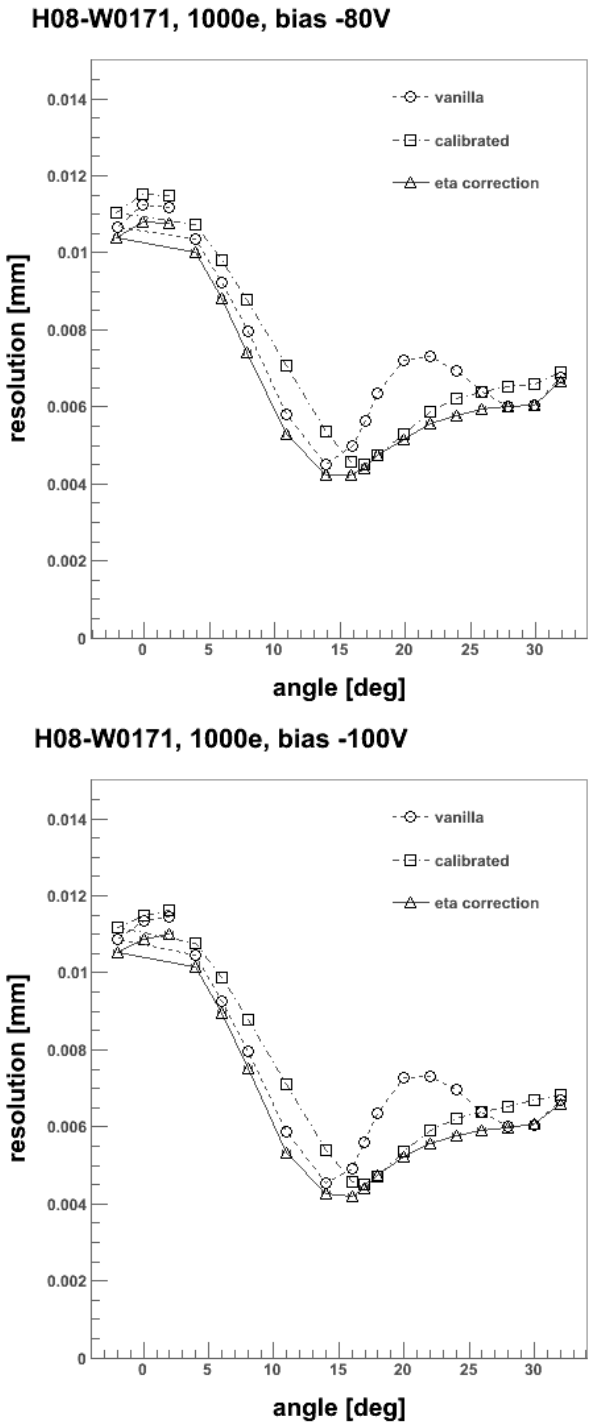

Figure 5.3. Spatial resolution versus angle for H08 device at four different reverse bias voltages: -40 V, -60 V, -80 V and -100 V.

5.2 EDGE STUDY

Data which was taken with the beam oriented near the edge of the test devices allows us to assess their performance in the periphery with higher statistics. Before calculating the track-matching efficiency, we examined the 2D distribution of number of hits per pixel. A strange effect which we observed was an inflamed penultimate row of pixels: the second to last row from the edge had an abnormal number of hits. This should be noted as a discontinuous “ridge” in the histogram even in light of the fact that the beam spot was centered near there. In Figure 5.4, this is shown on the left edge for the F08 device, and on the right edge for the H08 device. The reason why this occurs is not well understood. The effect suggests a disproportionate allocation of hits to the hyperactive row of pixels.

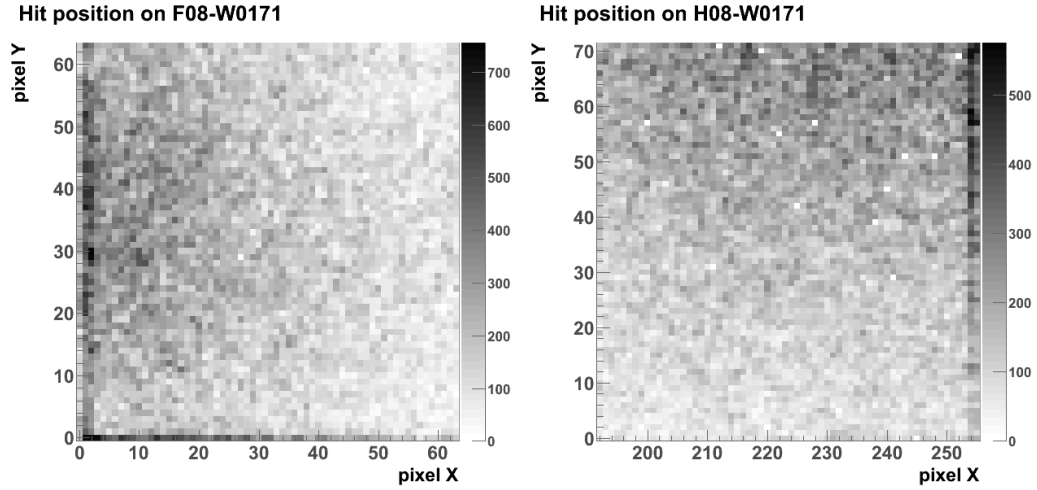

Figure 5.4. Distributions of pixel hit position for the F08 and H08 test devices. Note the inflamed row of pixels at the edge.

Our examination of the efficiency at the edge is testament to the effectiveness of the new edge technology of these sensors. Due to the participation of the active edge region in the charge collection process, the device continued to efficiently

match hits with tracks even past the last true row of pixels. A cross section of the 2D efficiency calculation was made near the edges and is shown in Figure 5.5. This forms a 1D distribution which can be fitted as a function of position to analyze the efficiency drop-off near the edge. Noting that the efficiency drop-off exhibits a sigmoidal shape, we used a surrogate function of the form

$$H(x) = 0.5\,\mathrm{erf}(\pm k[x - x_o]) + 0.5\,. \quad (7)$$

Having fit the function to the data at the edge of both devices, we then used the derived parameters to solve H(x) = 0.9, in order to obtain the distance from the edge of the chip where the device falls below 90% efficiency. According to this calculation, the F08 device falls below 90% efficiency at 12.3 μm from the edge of the chip, and the H08 device falls below 90% efficiency at 2.2 μm from the edge.

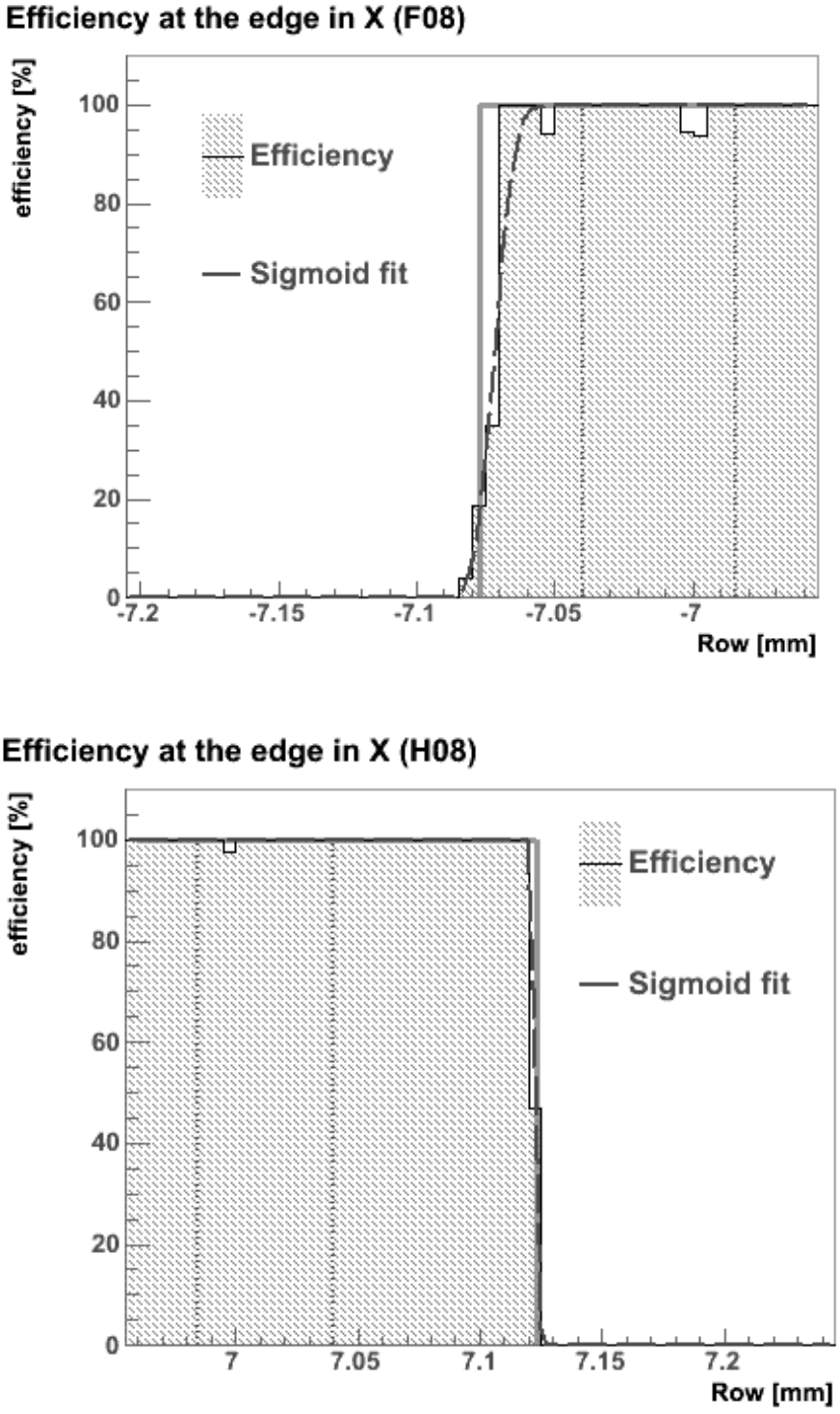

Figure 5.5. Efficiency near the edge of the F08 and H08 chips, fit with sigmoidal surrogate function.

6 CONCLUSION

We find that the silicon pixel sensor test devices perform in accordance with expectations and fulfill the technical needs of their intended implementation. The spatial granularity of this class of device is adequate for an implementation for an upgrade to the LHCb vertex detector or a similar experiment. The state-of-the-art active edge technology is effective in maximizing the useful area of the sensor with minimal drawbacks in the form of edge distortion effects. Beyond use in particle physics, edgeless silicon pixel detectors may also find a future in implementations for medical imaging or X-ray spectroscopy.

7 REFERENCES

1. K. Nakamura *et al.* (Particle Data Group), “2010 Review of Particle Physics.” J. Phys. G **37**, 075021 (2010)

2. P. Perez. (LHCb VELO Group) “The LHCb Vertex Locator performance and Vertex Locator upgrade.” arXiv:1209.4845 [physics.ins-det]

3. R. Turchetta. “Spatial resolution of silicon microstrip detectors.” Nucl. Instr. and Meth. A335 (1993) 44.

4. K. Akiba *et al*. “Charged Particle Tracking with the Timepix ASIC.” arXiv:1103.2739 [physics.ins-det]

5. J. Kalliopuska, J. Jakubek, L. Tlustos. “Overview on measured properties of VTT’s edgeless detectors and their use in high energy physics.” TIPP 2011

6. M. Bosma *et al.* “Edgeless planar semiconductor sensors for a Medipix3-based radiography detector.” 2011 JINST 6 C11019 doi:10.1088/1748-0221/6/11/C11019